Supplementary Information to

Modelling the gas–particle partitioning and water uptake of isoprene-derived secondary organic aerosol at high and low relative humidity

Dalrin Ampritta Amaladhasan[1], Claudia Heyn[2], Christopher R. Hoyle[2,3], Imad El Haddad[2], Miriam Elser[2,5], Simone M. Pieber[2,6], Jay G. Slowik[2], Antonio Amorim[7], Jonathan Duplissy[8,9], Sebastian Ehrhart[4,10], Vladimir Makhmutov[11], Ugo Molteni[2], Matti Rissanen[12], Yuri Stozhkov[11], Robert Wagner[8], Armin Hansel[13], Jasper Kirkby[4,14], Neil M. Donahue[15], Rainer Volkamer[16], Urs Baltensperger[2], Martin Gysel-Beer[2], and Andreas Zuend[1]

[1]Department of Atmospheric and Oceanic Sciences, McGill University, Montreal, Quebec, H3A 0B9, Canada
[2]Laboratory of Atmospheric Chemistry, Paul Scherrer Institute, 5232 Villigen PSI, Switzerland
[3]Institute for Atmospheric and Climate Science, ETH Zurich, 8092 Zurich, Switzerland
[4]CERN, 1211 Geneva, Switzerland
[5]Swiss Federal Laboratories for Materials Science and Technology, Automotive Powertrain Technologies, Dübendorf, Switzerland
[6]Empa, Laboratory for Air Pollution / Environmental Technology, Ueberlandstrasse 129, CH-8600 Dübendorf, Switzerland
[7]CENTRA and Faculdade de Ciencias, University of Lisbon, 1749-016 Lisbon, Portugal
[8]Institute for Atmospheric and Earth System Research (INAR) / Physics, University of Helsinki, 00014 Helsinki, Finland
[9]Helsinki Institute of Physics, University of Helsinki, 00014 Helsinki, Finland
[10]Finnish Environment Institute (SYKE), Marine Research Centre, 00790, Helsinki, Finland
[11]P.N. Lebedev Physical Institute of the Russian Academy of Sciences, 119991 Moscow, Russian Federation
[12]Aerosol Physics Laboratory, Physics Unit, Tampere University, Tampere, Finland
[13]Department of Ion Physics and Applied Physics, University of Innsbruck, 6020 Innsbruck, Austria
[14]Institute for Atmospheric and Environmental Sciences, Goethe University Frankfurt, 60438 Frankfurt am Main, Germany
[15]Center for Atmospheric Particle Studies, Carnegie Mellon University, Pittsburgh, PA 15213, USA
[16]Department of Chemistry & CIRES, University of Colorado at Boulder, Boulder, CO 80305 USA.

Correspondence to:
Dalrin Ampritta Amaladhasan (dalrin.amaladhasan@mail.mcgill.ca) or Andreas Zuend (andreas.zuend@mcgill.ca)

1 Pseudo-molar yields for early generation products

The pseudo-molar yields for the early generation products formed form the ozone-initiated oxidation of isoprene are obtained from the MCM-predicted molecular concentrations of the early-generation products and the hypothetical model tracer species "isoprene reacted". The used values are listed in Tables S1 and S2, representing different chamber conditions.

2 Total molar amounts of MCM species for the photooxidation of isoprene (Rastak et al., 2017) at 40 % RH and 25 °C

The total molar amounts in the gas and particle phases of the MCM species formed from the photooxidation of isoprene are shown in Table S3. These molar amounts have been used to predict the SOA concentration formed using the equilibrium partitioning model.

3 Comparison with other isoprene oxidation studies

3.1 Impact of varying RH on gas–particle partitioning for the ozonolysis study by Sato et al. (2013)

The model predicted SOA mass concentration for the ozonolysis of isoprene without an inorganic seed from low to high levels of water activity (1 – 99 % equilibrium RH) at similar experimental conditions as the ozonolysis study by Sato et al. (2013) is shown in the Fig. S1. The MCM-predicted system components and the surrogate species used were those from this study based on the CLOUD data from Fuchs (2017).

3.2 Impact of varying RH on gas–particle partitioning for the ozonolysis study by Clark et al. (2016)

Figure S2 shows the model predicted SOA mass concentrations and mass fractions of the components at varying levels of equilibrium RH (1 – 99 % RH) for similar experimental conditions as the ozonolysis study by Clark et al. (2016). The model SOA surrogate system used is that based on CLOUD data from Fuchs (2017) for the seed-free case.

3.3 Impact of varying RH on gas–particle partitioning for the ozonolysis study by Kleindienst et al. (2007) using ammonium sulfate seed (using CLOUD 9 scaling parameters for surrogate species)

Modelled SOA mass concentrations with an ammonium sulfate seed at varying levels of equilibrium RH under conditions similar to the ozonolysis study by Kleindienst et al. (2007) is shown in the Fig. S3. Corrected scaling parameters (scaled down to 55 % of the original values) have been used to calculate the molar yields of the higher generation species (see Table 3). Model system components based on the CLOUD data from the study by Fuchs (2017) have been used.

3.4 Impact of varying RH on gas–particle partitioning for the ozonolysis study by Kleindienst et al. (2007) using ammonium bisulfate seed

Modelled SOA mass concentrations with an ammonium bisulfate seed at varying levels of equilibrium RH under conditions similar to the ozonolysis study by Kleindienst et al. (2007) is shown in the Fig. S5. Corrected scaling parameters (scaled down to 55 % of the original values) have been used to calculate the molar yields of the higher generation species. Model system components based on the CLOUD data from the study by Fuchs (2017) have been used.

3.5 Impact of varying RH on gas–particle partitioning for 3.7 µg m^{-3} sulfuric acid seed at 25 °C

Modelled SOA mass concentrations in the presence of a sulfuric acid seed at varying water activity levels at a temperature of 25 °C are shown in Fig. S5. The CLOUD data based system components from Fuchs (2017) have been used for the model predictions. The scaling parameters for the surrogate components have been corrected / scaled down to 55 % of the original values to obtain model-measurement agreement for the SOA mass concentration at given levels of isoprene loading.

3.6 Impact of varying RH on gas–particle partitioning for the seed-free case of ozonolysis study by Fuchs (2017) using CLOUD 9 pseudo molar yields

Figure S6 shows the predicted equilibrium phase compositions as a function of water activity for the case without an inorganic seed from low to high levels of water activity. The modelled SOA mass concentrations are used for comparing the SOA yields for the sulfuric acid seeded case with that of the seed-free case with comparable gas phase chemistry and early generation product yields. The same pseudo-molar yields as the CLOUD 9 seeded cases have been used for all the system components along with corrections for the higher generation product yields (scaling the yields for the surrogate species to 55 % of the original values) were used for the model calculation (see Table 3).

3.7 Impact of varying RH on gas–particle partitioning for the ozonolysis study by Fuchs (2017) using sulfuric acid seed (using CLOUD 9 pseudo-molar yields)

Figure S7 shows the predicted equilibrium phase compositions as a function of water activity for the case with a sulfuric acid seed at 1.3 μg m^{-3} from low to high levels of water activity. The same amount of sulfuric acid seed as the ammonium bisulfate seed (see case 2 in Table 3) is used for comparison of SOA yield enhancement. The modelled SOA mass concentrations are used for comparing the SOA yield enhancement for the aerosol mixture with 3.7 μg m^{-3} of sulfuric acid seed (see case no. 3 in Table 3) and the aerosol mixture with 1.3 μg m^{-3} of sulfuric acid seed (see case no. 4 in Table 3). The same pseudo-molar yields as the CLOUD 9 seeded cases have been used for all the system components along with corrections for the higher generation product yields (scaling the yields for the surrogate species by 55 %) were used for the model calculation.

3.8 Impact of varying RH on the total organic components for the study by Fuchs (2017) using sulfuric acid seed and ammonium bisulfate seed (using CLOUD 9 pseudo-molar yields)

Figure S8a,b shows the total concentration of organic components in the PM phase as a function of water activity (bulk equilibrium RH) using sulfuric acid seed (a) or ammonium bisulfate seed (b). In the presence of sulfuric acid seed, the model predicts already high levels of PM organic mass concentration at low to intermediate RH levels followed by very little increase in PM mass concentration towards high RH levels, shown by the solid green line in Fig. S8a. The dashed lines in this Fig. provide the corresponding prediction for the seed-free case under otherwise equivalent simulation conditions.

References

Clark, C. H., Kacarab, M., Nakao, S., Asa-Awuku, A., Sato, K., and Cocker III, D. R.: Temperature effects on secondary organic aerosol (SOA) from the dark ozonolysis and photo-oxidation of isoprene, Environmental science & technology, 50, 5564-5571, 2016.

Fuchs, C.: Investigation of the role of SO_2 and isoprene in aqueous phase secondary aerosol formation, PhD, ETH Zurich, Zurich, 177 pp., 2017.

Kleindienst, T. E., Lewandowski, M., Offenberg, J. H., Jaoui, M., and Edney, E. O.: Ozone-isoprene reaction: Re-examination of the formation of secondary organic aerosol, Geophysical Research Letters, 34, 2007.

Nakayama, T., Sato, K., Imamura, T., and Matsumi, Y.: Effect of Oxidation Process on Complex Refractive Index of Secondary Organic Aerosol Generated from Isoprene, Environmental science & technology, 52, 2566-2574, 2018.

Rastak, N., Pajunoja, A., Acosta Navarro, J. C., Ma, J., Song, M., Partridge, D. G., Kirkevåg, A., Leong, Y., Hu, W., and Taylor, N.: Microphysical explanation of the RH-dependent water affinity of biogenic organic aerosol and its importance for climate, Geophysical Research Letters, 44, 5167-5177, 2017.

Sato, K., Inomata, S., Xing, J.-H., Imamura, T., Uchida, R., Fukuda, S., Nakagawa, K., Hirokawa, J., Okumura, M., and Tohno, S.: Effect of OH radical scavengers on secondary organic aerosol formation from reactions of isoprene with ozone, Atmospheric environment, 79, 147-154, 2013.

Surratt, J. D., Chan, A. W., Eddingsaas, N. C., Chan, M., Loza, C. L., Kwan, A. J., Hersey, S. P., Flagan, R. C., Wennberg, P. O., and Seinfeld, J. H.: Reactive intermediates revealed in secondary organic aerosol formation from isoprene, Proceedings of the National Academy of Sciences, 107, 6640-6645, 2010.

Table S1. CLOUD 10 seed-free case at 5 °C and ~1013 hPa chamber pressure.

MCM species name	Pseudo-molar yield [a]
Glyoxal	2.91918E-03
Methylglyoxal	1.72751E-02
Methyl vinyl ketone	2.24310E-01
MACO3H	2.75736E-01
MACROOH	3.50011E-04
HMACROOH	2.47619E-07

[a] Pseudo-molar yield is the ratio of the molecular concentration of the MCM-predicted species formed per molecular concentration of the tracer species "isoprene reacted". It is a dimensionless quantity.

5

Table S2. CLOUD 9 inorganic seeded cases with ammonium bisulfate or sulfuric acid seed particles at 10 °C and ~1233 hPa chamber pressure.

MCM species name	Pseudo-molar yield
Glyoxal	5.4621E-03
Methylglyoxal	3.1898E-02
Methyl vinyl ketone	2.3956E-01
MACO3H	2.8100E-01
MACROOH	5.1857E-04
HMACROOH	5.6252E-07

Table S3. Total molar concentrations of the MCM species from the photooxidation of isoprene used with the AIOMFAC-based gas–particle partitioning model for a target amount of ~ 3.6 μg m^{-3} SOA mass concentration at 40 % RH.

MCM species name	$\mathbf{n^t}$ (mol m^{-3}) [a]
IEB1OOH	2.3613E-08
IEB2OOH	1.9473E-08
C59OOH	1.6253E-08
IEC1OOH	5.6733E-09
C58OOH	2.4533E-09
IEPOXA	2.9237E-09
C57OOH	1.9933E-09
IEPOXC	1.2669E-09
HIEB1OOH	5.5422E-10
INDOOH	4.0863E-10
IEACO3H	4.6622E-10
C525OOH	4.1566E-10
HIEB2OOH	2.7711E-10
IEC2OOH	3.1081E-10
INAOOH	2.3350E-10
C510OOH	1.7692E-10
INB1OOH	1.1675E-10
IECCO3H	1.5541E-10
INCOOH	5.8376E-11
INB2OOH	5.8376E-11
2-methyltetrol dimer[b]	9.0452E-09

[a] Total molar amounts (gas and particle phase)

[b] 2-methyltetrol dimer was suggested by Surratt et al. (2010) and included in the photooxidation of isoprene MCM-based surrogate system by Rastak et al. (2017).

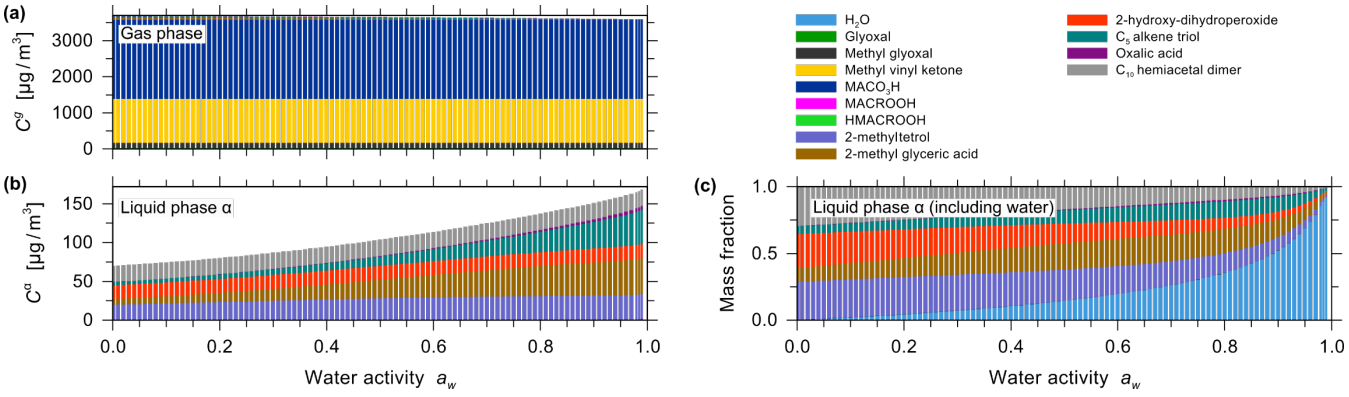

Figure S1. Predicted mass concentrations of the components (shown stacked; excluding water) for the seed-free case of ozone-initiated isoprene oxidation in (a) the gas phase and (b) the single liquid particle phase present. (c) The mass fractions in the liquid phase including water. All for 1 % to 99 % water activity (equilibrium RH) and a reacted isoprene concentration of 5484 µg m^{-3} at 25 °C.

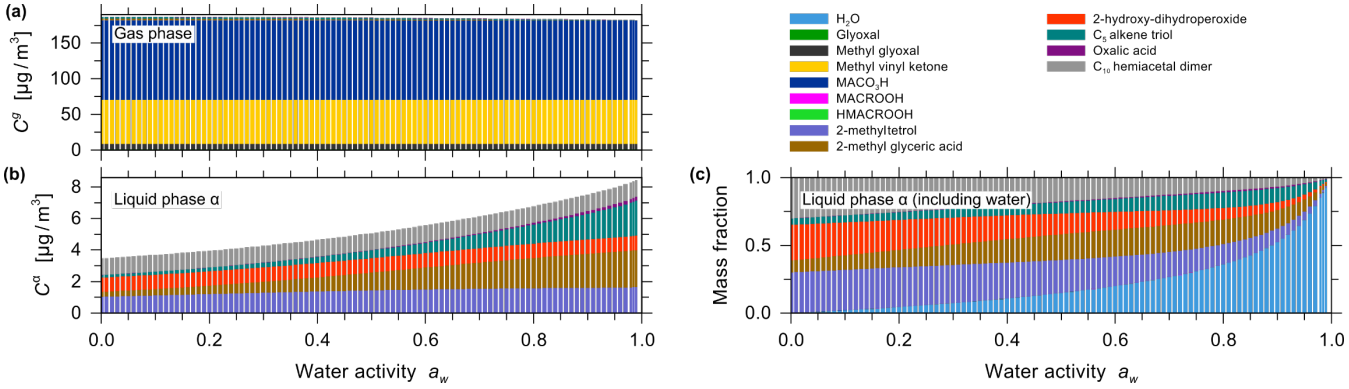

Figure S2. Predicted mass concentrations of the components (shown stacked; excluding water) for the seed-free case of ozone-initiated isoprene oxidation in (a) the gas phase and (b) the single liquid particle phase present. (c) The mass fractions in the liquid phase including water. All for 1 % to 99 % water activity (equilibrium RH) and a reacted isoprene concentration of 278 µg m^{-3} at 5 °C.

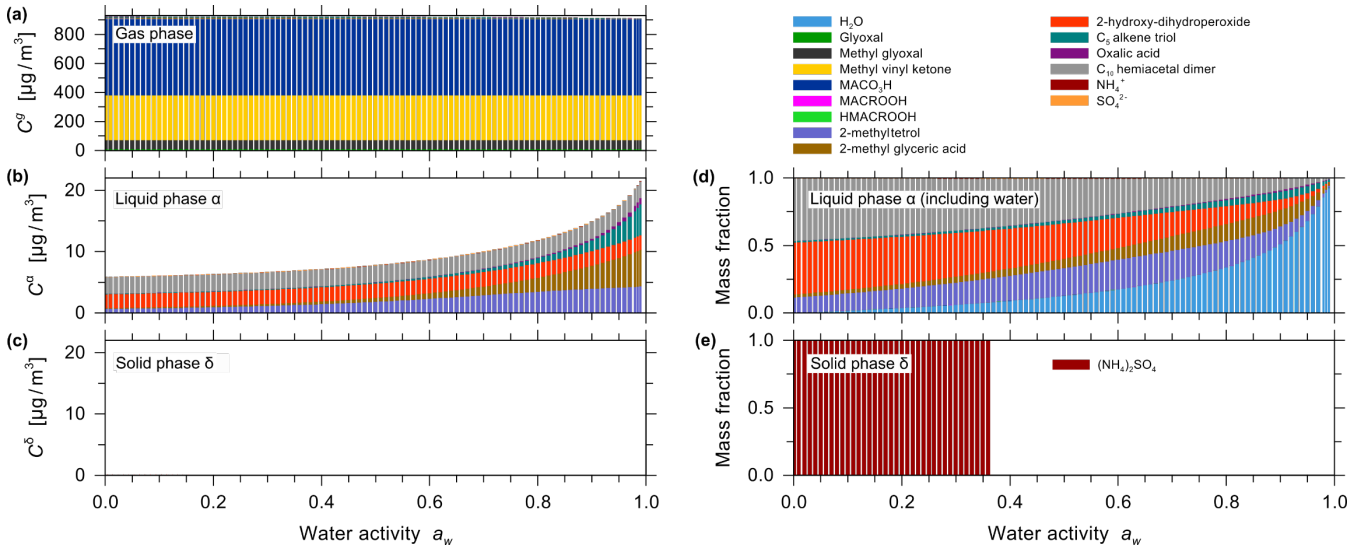

Figure S3. Predicted equilibrium gas phase (a) and liquid phase (b) mass concentrations for a reacted isoprene concentration of 1270 µg m^{-3} at 22 °C, 0.05 µg m^{-3} of ammonium sulfate seed and variable water content (1 % to 99 % water activity). Using the same corrected scaling parameters for calculating the molar yields of higher generation species as for the CLOUD 9 seeded cases. The predicted phase compositions shown in (a) and (b) are exclusive of the water content. (c) The solid-phase concentrations of ammonium sulfate (≤ 0.05 µg m^{-3}), where present, are very small on the shown scale compared to the organic mass concentrations in (b). (d) Mass fractions in the liquid phase α and (e) the solid ammonium sulfate phase δ (where present). Shown in panels (a), (b), (c) are phase-specific mass concentrations for a humidification scenario, with deliquescence of ammonium sulfate predicted to occur at $a_w \approx 0.36$ and solid–liquid equilibrium below that water activity level. Here the deliquescence point of this salt is relatively low compared to pure ammonium sulfate (+ water) due to the low salt mass fraction and related dilution by the organic compounds and water.

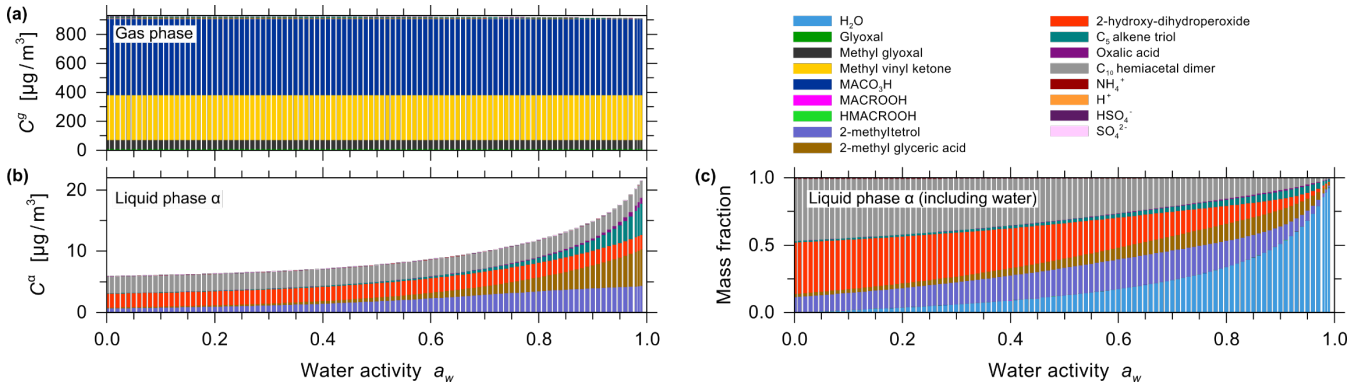

Figure S4. Predicted equilibrium gas phase (a) and liquid phase (b) mass concentrations for a reacted isoprene concentration of 1270 µg m^{-3} at 22 °C, 0.05 µg m^{-3} of ammonium bisulfate seed and variable water content (0 % to 99 % water activity. The predicted phase compositions shown in (a) and (b) are exclusive of the water content. (c) Mass fractions in the liquid phase α, including water content.

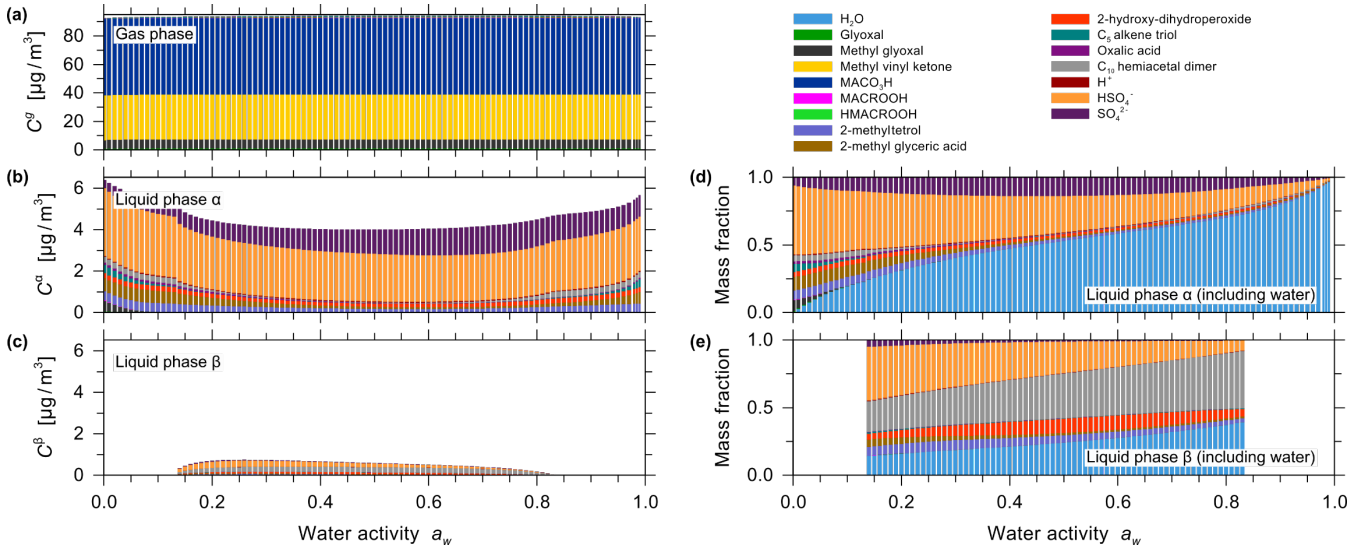

Figure S5. Predicted equilibrium gas phase (a) and liquid phase (b, c) mass concentrations for a reacted isoprene concentration of 130 µg m^{-3} at 25 °C, 3.7 µg m^{-3} of sulfuric acid seed and variable water content (0 % to 99 % water activity). The predicted phase compositions shown in (a) to (c) are exclusive of the water content. (d, e) Mass fractions in the liquid phases α and β, including water content.

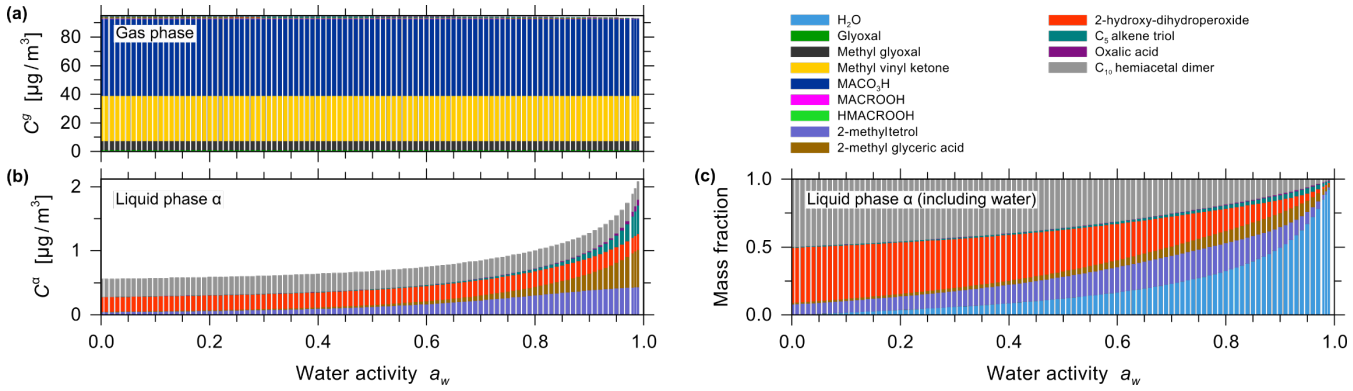

Figure S6. Predicted equilibrium gas phase (a) and liquid phase (b) mass concentrations for a reacted isoprene concentration of 130 µg m^{-3} at 10 °C, seed-free case and variable water content (1 % to 99 % water activity). Pseudo-molar yields from the CLOUD 9 case were used for all system components (i.e. with scaling factor applied relative to CLOUD 10 case). The predicted phase compositions shown in (a) and (b) are exclusive of the water content. (c) Mass fraction in the liquid phase α including water content.

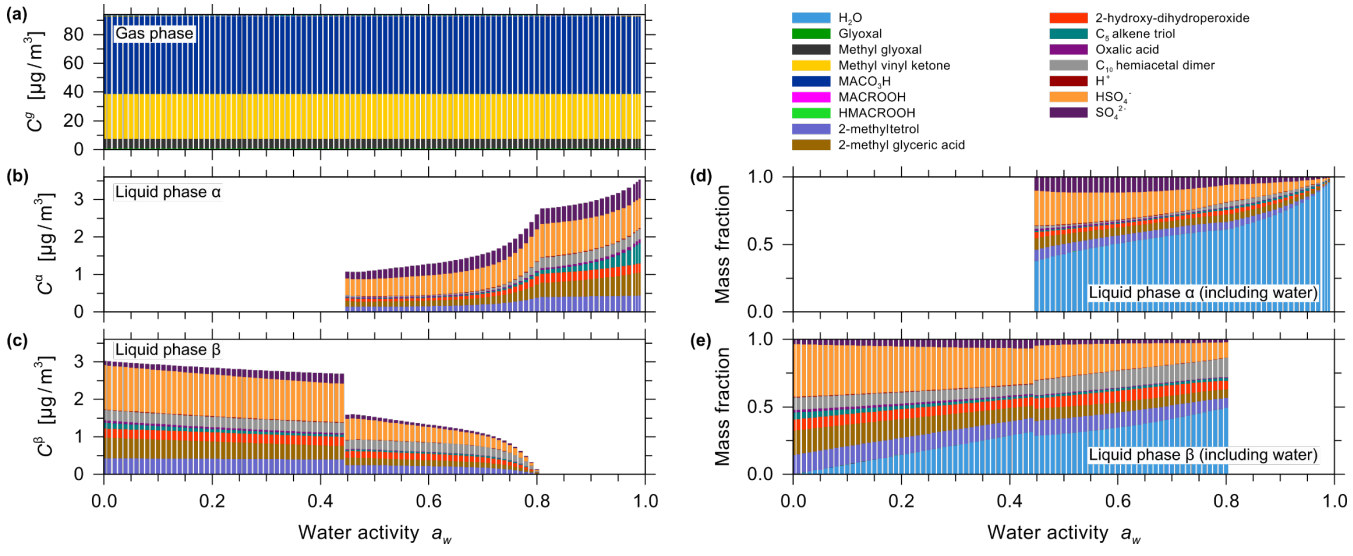

Figure S7. Predicted equilibrium gas phase (a) and liquid phase (b, c) mass concentrations for a reacted isoprene concentration of 130 µg m^{-3} at 10 °C, 1.3 µg m^{-3} of sulfuric acid seed and variable water content (1 % to 99 % water activity). The predicted phase compositions shown in (a) to (c) are exclusive of the water content. (d, e) Mass fractions in the liquid phases α and β, including water content.

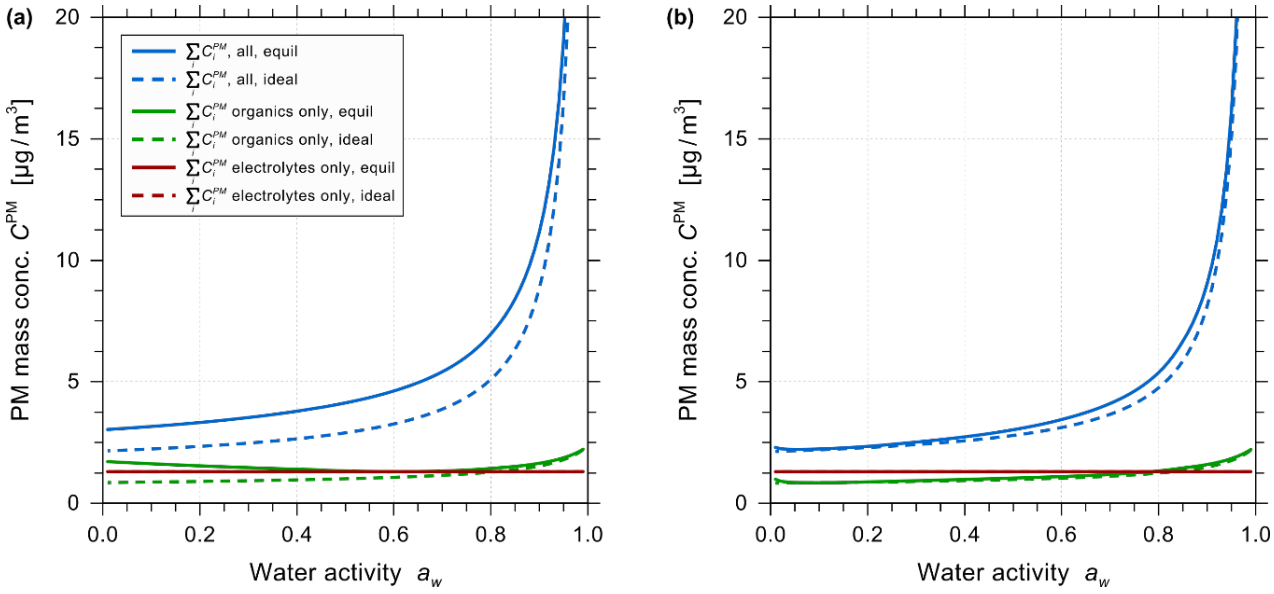

Figure S8. Predicted equilibrium total PM and total organic PM mass concentrations for a reacted isoprene concentration of 130 µg m^{-3} at 10 °C, with (a) 1.3 µg m^{-3} of sulfuric acid seed or (b) 1.3 µg m^{-3} of ammonium bisulfate seed at variable water content (0.1 % to 99 % water activity). Solid lines show the model predictions for the AIOMFAC-based equilibrium partitioning case and the dashed lines show the model predictions for equilibrium partitioning assuming ideal mixing.

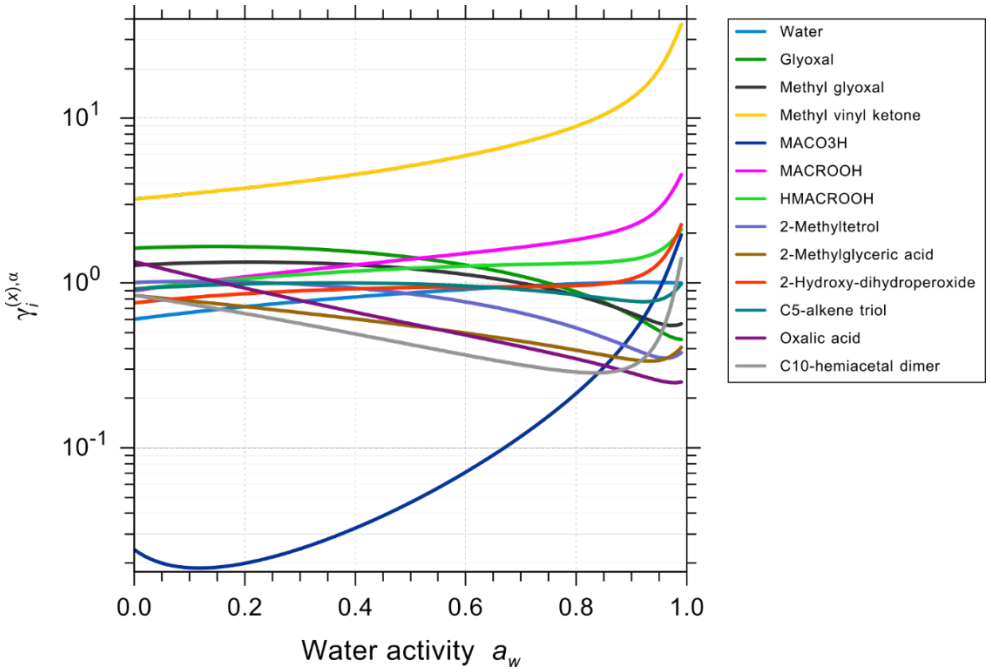

Figure S9. Predicted mole-fraction-based activity coefficients of water and the organic compounds for the seed-free isoprene oxidation system shown in Fig. 4 of the main text; see further details there. An activity coefficient of 1 indicates ideal mixing on mole fraction basis.

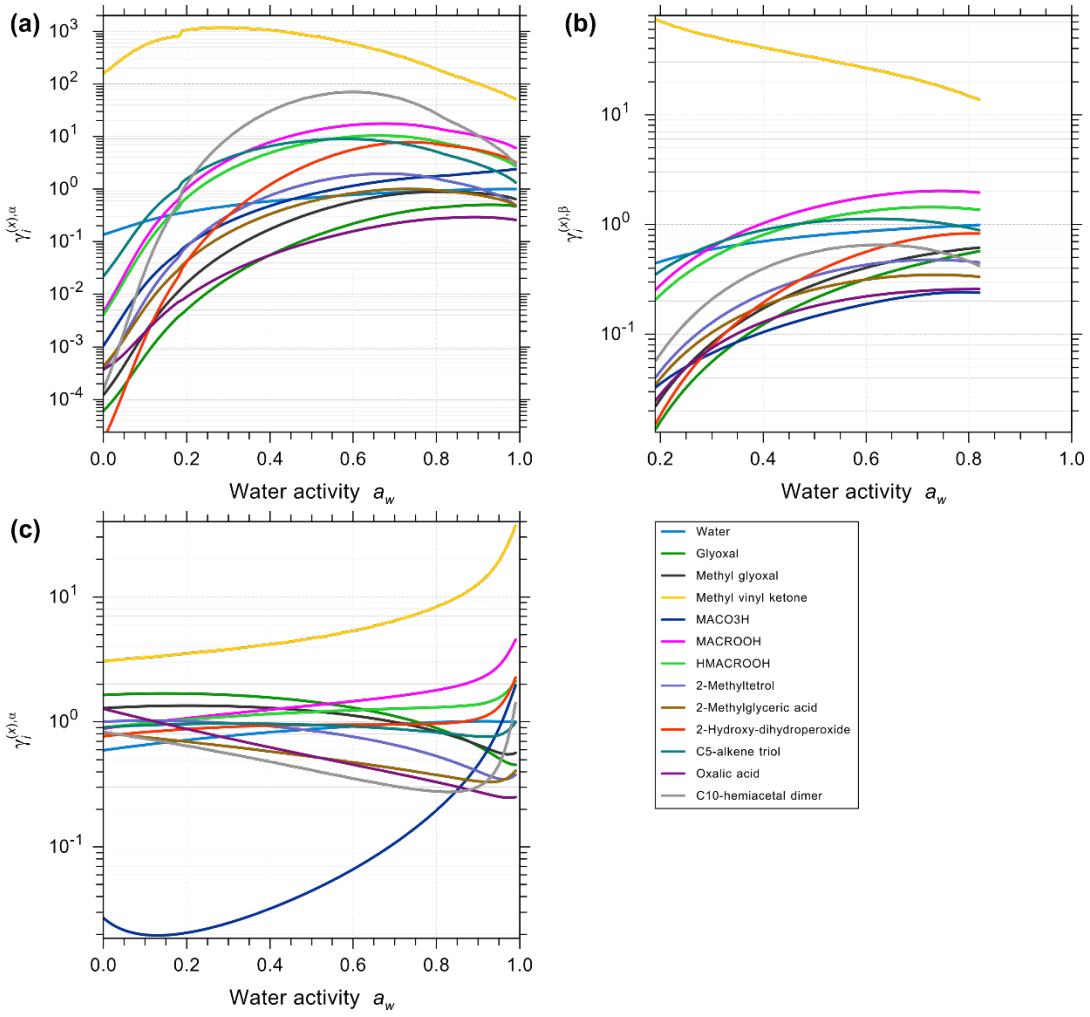

Figure S10. Predicted mole-fraction-based activity coefficients of water and the organic compounds for an isoprene oxidation system with (**a**, **b**) 3.7 µg m^{-3} sulfuric acid seed (similar to system of Fig. S5 but here at 10 °C) and (**c**) the corresponding seed-free case (for the system shown in Fig. S6). The reacted isoprene concentration was 130 µg m^{-3} at 10 °C in both cases. Pseudo-molar yields determined by the CLOUD 9 case were consistently used for all system components (i.e. with scaling factor applied relative to CLOUD 10 case). (a) The activity coefficients in the aqueous, sulfuric acid rich phase α (not showing activity coefficients of inorganic ions). (b) The activity coefficients in organic-rich phase β shown for the water activity range where this phase coexists with phase α. Only a single phase exists in the seed-free case (c). Note the different ordinate scales.